

Spin-orbit coupling controlling the superconducting dome of artificial superlattices of quantum wells

Maria Vittoria Mazziotti*

*INFN, Laboratori Nazionali di Frascati, Via Enrico Fermi 40, Roma, Italy and
Rome International Center for Materials Science, Superstripes,
RICMASS, Via dei Sabelli 119A, 00185 Roma, Italy*

Antonio Bianconi

*Rome International Center for Materials Science,
Superstripes RICMASS Via dei Sabelli 119A, 00185 Roma, Italy and
Istituto di Cristallografia - Consiglio Nazionale delle Ricerche IC-CNR,
via Salaria Km 29.300, Monterotondo (Roma) I-00016, Italy*

Roberto Raimondi

Dipartimento di Matematica e Fisica, Università Roma Tre, via della Vasca Navale 84 00146 Roma, Italy

Gaetano Campi

*Istituto di Cristallografia - Consiglio Nazionale delle Ricerche IC-CNR,
via Salaria Km 29. 300, Monterotondo (Roma) I-00016, Italy*

Antonio Valletta

*Institute for Microelectronics and Microsystems IMM,
Italian National Research Council CNR, via del Fosso del Cavaliere, 100, 00133 Roma, Italy
(Dated: November 22, 2022)*

While it is known that a resonant amplification of T_c in two-gap superconductors can be driven by using the Fano-Feshbach resonance tuning the chemical potential near a Lifshitz transition, little is known on tuning the T_c resonance by cooperative interplay of the Rashba spin-orbit coupling (RSOC) joint with phonon mediated (e-ph) pairing at selected k-space spots. Here we present first-principles quantum calculation of superconductivity in an artificial heterostructure of metallic quantum wells with 3 nm period where quantum size effects give two-gap superconductivity with RSOC controlled by the internal electric field at the interface between the nanoscale metallic layers intercalated by insulating spacer layers. The key results of this work show that fundamental quantum mechanics effects including RSCO at the nanoscale (Mazziotti et al Phys. Rev. B, 103, 024523, 2021) provide key tools in applied physics for quantitative material design of unconventional high temperature superconductors at ambient pressure. We discuss the superconducting domes where T_c is a function of either the Lifshitz parameter (η) measuring the distance from the topological Lifshitz transition for the appearing of a new small Fermi surface due to quantum size effects with finite spin-orbit coupling and the variable e-ph coupling g in the appearing second Fermi surface linked with the energy softening of the cut off ω_0 .

I. INTRODUCTION

While in the early times fundamental studies on quantum size effects in artificial superlattices (SLs) of quantum wells have been limited by technological constraints to a thickness of hundreds of nanometers [1], now the electronics industry is focusing toward devices with 3 nm technology. Recently, artificial superlattices of atomically thin layers down to the few nanometers scale have been synthesized [2–8]. The control of quantum size effects at the nanometer level led to advances in understanding fundamental physical phenomena at nanoscale and to the realisation of novel functional devices. The electronic properties of these devices can be modified not only by

a careful selection of the materials and the thickness of quantum units within the stack, but also by tuning the charge density, the spacer layers, the misfit strain and relative orientation of the layers. Recently, there has been a growing interest in the design of superlattices of quantum wells, where stacks of first units of nanometer thick superconducting layers are intercalated by nanoscale insulating layers following the European patent on the design of artificial high- T_c atomic-limit superconducting heterostructures [9] and the US patent [10] for the T_c -resonant amplification via Fano-Feshbach resonance. The possibility of T_c amplification by Fano-Feshbach resonance between open and close pairing channels in artificial superlattices showing two-gap superconductivity was confirmed by the discovery of naturally layered two-gap superconductors like doped MgB_2 in 2001, doped iron-based superconductors in 2008, and oxide-oxide perovskite interfaces, which have inspired the material design of different classes of

* Corresponding author. E-mail: vittoria.mazziotti@gmail.com

artificial nanoscale superlattices [11–13]. While two-gap superconductivity in the twentieth century was considered a theoretical curiosity of mathematical physics, in layered systems it has become a hot topic in the first two decades of this century. The classical theory of two-gap superconductivity was first developed by introducing the pair exchange between two BCS condensates in the weak coupling regime by Moskalenko [14] and Suhl, Matthias and Walker (SMW), [15]. A second theoretical approach, the multi-band Migdal-Eliashberg theory, extended the theory to the case where one of the two condensates is in the strong coupling regime as was applied, for example, in doped MgB_2 [16 and 17]. The third theoretical approach available to understand two-gap superconductivity was the mixed boson-fermion model [18], derived from the Tomonaga theory of pions cloud in nuclear matter [19] and the the negative-U-centers model where localised bosons or bipolarons interact symbiotically with free particles in different parts of the unit cell, proposed for heavy fermions [20] and doped $BaBiO_3$ [21 and 22]. A fourth approach, proposed by Bianconi, Perali and Valletta (BPV) [23–25] provides the theory of two-gap superconductivity for the scenario where a first BCS pairing scattering channel (open channel) in a first Fermi surface resonates with a second pairing channel (closed channel) in the BCS-BEC crossover regime in the second Fermi surface [26–41].

While it is known that the BCS superconductivity theory predicts that T_c does not depend on the variation of the Fermi level, assumed to be very far from the band edge, in the BPV two-gap superconductors the second Fermi surface is at a finite particular distance from the band edge. In fact the resonant T_c -amplification strongly depends on the relative position of the chemical potential with respect to the topological Lifshitz transition for the second Fermi surface appearance. Therefore T_c is a function of the Lifshitz parameter η defined as

$$\eta = \frac{\mu - E_L}{\Delta E}, \quad (1)$$

where μ is the chemical potential, E_L is the second subband bottom energy and ΔE is the dispersion along the z direction of the highest-energy subband. In the specific superlattice studied here $\Delta E=30$ meV.

Above the Lifshitz transition for a new Fermi surface appearance, T_c as a function of η shows a quantum resonance between open and closed scattering channels discovered by Fano [42]. Such so-called Fano-Feshbach resonance was later found in X-ray spectroscopy [43–45], in quantum devices [46–48], and quantum optics [48], shape resonance in nuclear physics [49] and in the early works in two-gap superconductivity [23–25], and Feshbach resonance in ultra cold gases [50]. For a historical perspective see Ref.[51]. The key feature of the BPV theory is the calculation of the energy dependent pair-transfer exchange interaction, which generates the Fano-Feshbach resonance in the Bogoliubov multi-gap superconductivity theory [52] [53]. The energy dependent pair-transfer

exchange term is calculated from the overlap of the four wave-functions of the two-electron pairs at the two Fermi levels as obtained from the solution of the Schrödinger equation [11, 12, 25–28, 54–60] or the Dirac equation [61] for the particular nanoscale superlattice in the real space. This provides the line-shape of the T_c amplification by Fano-Feshbach resonance due to configuration interaction between different pairing channels in the two-gap superconductivity in artificial superlattices of quantum wires and quantum wells which is missing in the single-gap BCS theory. The T_c amplification as function of Lifshitz parameter shows the typical Fano line-shape resonance with a dip at the Fano antiresonance near $\eta=0$ and a maximum amplification of T_c for η in the range 1 – 1.5. In superlattices of quantum wells the topological Lifshitz transition from a closed 3D Fermi surface to an open corrugated cylindrical Fermi surface, called opening a neck, occurs at $\eta=1$ with only a singular critical point in the k-space, which is not enough to produce a peak in the density of states. Recently it has been reported that it is possible to get a further amplification of the critical temperature T_c for superconductivity in a two-band two-gap superconductor by including spin orbit interaction [61].

In this scenario the quantum calculation of the energy dependent pair-transfer exchange term requires the solution of the Dirac equation for the superlattice. The RSOC was proposed to be controlled by the internal electric field E at the interface between nanometer thick metallic layers intercalated by insulating layers forming the heterostructure at atomic limit. In the presence of RSOC the T_c shows a maximum at the topological Lifshitz transition from a *torus* to a corrugated *cylinder* associated with an unconventional higher order van Hove singularity (VHS) associated with a circular line of critical points and a sharp peak in the DOS increasing with RSOC strength[61].

The maximum critical temperature in the curves T_c versus η occurs at η near 1 and electron-phonon coupling ($g = 0.4$) in the second subband and weak coupling ($g=0.1$) in the first subband [61]. However the role of the electron-phonon coupling in the small appearing Fermi surface in the Fano-Feshbach resonance remains elusive. In fact large variations of the electron-phonon interactions with the chemical potential, due to the emergence of a Kohn anomaly at particular spots in the k-space, was experimentally determined in the archetypal case of two-gap layered alloy $Mg_{1-x}Al_xB_2$ by Simonelli et al. [62 and 63]. While it is known that the critical temperature as a function of doping and electron-phonon interaction in several families of high-temperature superconductors shows a 3D phase diagram [64–67], the superconducting *dome* remains elusive.

In this work we fill this gap by first-principle calculations of the resonant superconducting domes for the two-gap resonant superconductivity in the artificial superlattice introduced above. We include the energy dependent intra-band electron-phonon coupling for electrons in the

upper subband forming the appearing Fermi surface. We report the superconducting dome in a 3D color-plot for T_c as a function of two parameters, i.e. (i) the Lifshitz parameter measuring the position of the chemical potential relative to the Lifshitz transition and (ii) the strength of the electron-phonon interaction in the upper subband in the absence and in the presence of increasing RSOC. As we shall see the top of the superconducting dome is given by the Fano-Feshbach resonance driven by quantum configuration interaction between open and closed pairing channels, i.e., between a first gap in the BCS regime, resonating with a second gap in the BCS-BEC crossover regime. We show that the maximum T_c increases with increasing RSOC interaction and we propose the possible pathway in the (η) and g plain due joint variation of doping and strain inspired by experimental data on Al doped MgB_2

II. RESULTS AND DISCUSSION

A. Fano-Feshbach resonance

The proposed heterostructure has periodicity $d = 30$ Å and is made of alternating superconducting layers of thickness $L = 23$ Å and insulating layers of thickness $W = 7$ Å. The insulating layers are realized with a potential barrier $V = 0.5$ eV as shown in Fig. 1. This is a selected a prototype of an artificial superlattice of nanoscale quantum wells made of a conventional superconductor intercalated by insulating layers where the tunneling of the electrons through the barrier is of the order of the energy cut-off of the pairing interaction. The particular case discussed in this work provides a typical example which grabs the essential physics for practical realizations of artificial nanoscale heterostructures made of quantum superlattices with period in the range of between 1.5 and 4 nm.

Whereas along the stacking direction z the electrons experience a periodic potential, they are free in the xy plane. As a result, the non-interacting single-particle wave functions are given by

$$\psi_{n\mathbf{k}\lambda}(\mathbf{r}) = \varphi_{nk_z}(z) \frac{e^{i\mathbf{k}_{\parallel}\cdot\mathbf{r}_{\parallel}}}{\sqrt{\mathcal{A}}} \chi_{\lambda}(\theta_{\mathbf{k}_{\parallel}}), \quad (2)$$

where the wave vector components $\mathbf{k} = (k_x, k_y, k_z) \equiv (\mathbf{k}_{\parallel}, k_z)$ label plane waves in the xy plane of area \mathcal{A} and the Bloch functions $\varphi_{nk_z}(z)$ along the z axis, n being a subband index and $\lambda = \pm 1$ the helicity index. In the above $\theta_{\mathbf{k}_{\parallel}}$ is defined as the angle between the \mathbf{k}_{\parallel} wavevector and the k_x axis. The functions $\varphi_{nk_z}(z)$ and the corresponding eigenvalues are obtained by imposing the continuity of the wave function and its first derivative at the discontinuity points of the potential. Finally, $\chi_{\lambda}(\theta_{\mathbf{k}_{\parallel}})$ are the spinors which are the eigenstates of the Rashba spin-orbit coupling. In the following the attractive interaction will be projected in the Rashba eigenstates as done

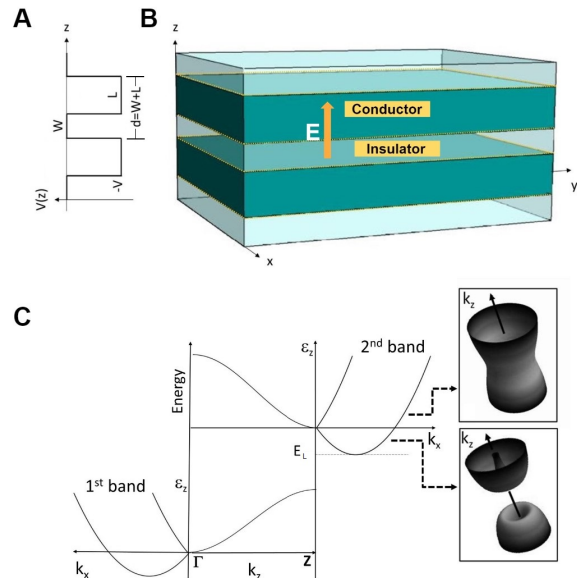


Figure 1. Pictorial view of the 3 nm superlattice of quantum wells studied in this work. The panel A shows the periodic potential along the z -direction where the electrons are confined in the metallic layers of thickness $L = 2.3$ nm (dark green layers in panel B) separated by the potential barrier of width $W = 0.7$ nm made of insulating layers (light green in panel B). In this nanoscale superlattice an internal electric-field, \mathbf{E} , is present which makes possible a Rashba coupling for the electron gas in the thin metallic layers. Panel C: the dispersion of the first two superlattice subbands are shown along k_x and k_z in the presence of the RSOC. The RSOC shifts the bottom of the second subband at E_L by an amount E_0 defined in the main text. In the panels on the right we have plotted the Fermi surfaces for the negative helicity subband above and below the anomalous van Hove singularity due to the spin-orbit coupling. The intensity of the gap, Δ_2 , in the second subband increases going from dark to light colour.

in Ref.[68]. Then, in this 3 nm superlattice the quantum size effects split the electronic spectrum in n -subbands. In the following we focus in two-gap superconductivity where the chemical potential is tuned by strain or charge density near the band edge of the second, $n = 2$, subband [11–13, 23–29, 31–36, 60, 69–71] including the Rashba spin orbit coupling [61, 68, 72–77].

In agreement with Ref.[61] the Rashba coupling constant is described by the following equation:

$$\alpha = 2 \frac{\hbar^2}{2m} \frac{2\pi}{d} \alpha_{SO}, \quad (3)$$

where α_{SO} is a dimensionless parameter that describes the strength of the Rashba coupling in units of the modulation parameter of the superlattice d and in the numerical evaluation we will use units such that the effective mass m will be fixed to one. Then, it is possible to change the relative intensity of the Rashba coupling by changing the periodicity of the superlattice.

The spin-orbit coupling induces a Lifshitz transition

[61] associated with a particular unconventional van Hove singular point [78–80] in the negative helicity states (we recall that the RSOC breaks the spin degeneracy yielding two helicity states at fixed wavevector \mathbf{k}), forming a circle whose radius increases with the RSOC strength. Notice that the RSOC shifts the bottom edge E_L by an amount $E_0 = -(m\alpha^2)/(2\hbar^2)$. When the Lifshitz parameter, defined in Eq.(1), will be used in the presence of RSOC, it is understood that the bottom edge E_L is shifted by the above amount E_0 . The amplification of the gaps and T_c increases when the chemical potential is tuned around an unconventional Lifshitz transition. Therefore in addition to the Cooper coupling, we take into account the key role of the Fano-Feshbach due to configuration interaction in the equation of the gap by evaluating the exchange interaction between pairs of singlets in subbands with different quantum numbers and different helicity.

The two-gap equations for the superlattice need to include the contact exchange interaction connecting pairs in different bands with different helicity of the pairing. The pair $\{(n, \mathbf{k}, \lambda), (n, -\mathbf{k}, \lambda)\}$ can be scattered into the pair $\{(n', \mathbf{k}', \nu), (n', -\mathbf{k}', \nu)\}$ where n and n' are the band indices, \mathbf{k} and \mathbf{k}' are the wave-vectors and λ and ν are the helicity indices. By recalling the results of previous work (see Ref. [61]), the zero-temperature two-gap equations read:

$$\Delta_{\lambda,n}(\mathbf{k}) = \lambda e^{i\theta_{\mathbf{k}}}_{\parallel} \Delta_n(k_z), \quad (4)$$

$$\Delta_n(k_z) = -\frac{U_0}{2} \sum'_{n',k'_z} I_{nk_z,n'k'_z} \Delta_{n'}(k'_z) \sum'_{\nu,\mathbf{k}'_{\parallel}} \frac{1}{2E_{n',\nu,\mathbf{k}'}} ,$$

where the quasiparticle energy, in the superconducting state, is

$$E_{n',\nu,\mathbf{k}'} = \sqrt{(\varepsilon_{\nu\mathbf{k}'_{\parallel}} + \varepsilon_{n'k'_z} - E_F)^2 + |\Delta_{n'}(k'_z)|^2}, \quad (5)$$

being understood that $\mathbf{k}' = (k'_x, k'_y, k_z) \equiv (\mathbf{k}'_{\parallel}, k'_z)$. The presence of RSOC affects only the in-plane part of the wave functions: hence, it is convenient to indicate the eigenvalues of the single-particle non-interacting Hamiltonian with the sum $\varepsilon_{\nu\mathbf{k}'_{\parallel}} + \varepsilon_{n'k'_z}$, where $\varepsilon_{\nu\mathbf{k}'_{\parallel}} = \hbar\mathbf{k}'_{\parallel}{}^2/(2m) + \lambda\alpha k'_{\parallel}$ and $\varepsilon_{n'k'_z}$ is given by the numerical solution of the Kroenig-Penney like problem in the z direction. The primed sums in Eq.(5) indicate that we consider only the pairs whose energies differ from the Fermi energy less than the renormalized cut-off Debye energy, i.e. $|\varepsilon_{\nu\mathbf{k}'_{\parallel}} + \varepsilon_{n'k'_z} - E_F| < \omega_0$. Finally, in Eq.(5) the important exchange integral $I_{nk_z,n'k'_z}$, which carries the information of the motion along the z axis, reads

$$I_{nk_z,n'k'_z} = \frac{2\pi}{L_{\parallel}^2} \int |\varphi_{n,k_z}(z)|^2 |\varphi_{n',k'_z}(z)|^2 dz. \quad (6)$$

One notices in Eq.(4) that the pairing potential depends linearly on the helicity index λ and through a phase factor on the in-plane momentum, whereas the quantity $\Delta_n(k_z)$ does not depend explicitly on both in-plane momentum and helicity [68]. To obtain the critical temperature we need to consider the finite-temperature version

of the two-gap equations of Eq.(5), which is

$$\Delta_n(k_z) = -\frac{U_0}{2} \sum'_{n',k'_z} I_{nk_z,n'k'_z} \Delta_{n'}(k'_z) \sum'_{\nu,\mathbf{k}'_{\parallel}} \frac{\tanh(\frac{\beta E_{n',\nu,\mathbf{k}'}}{2})}{2E_{n',\nu,\mathbf{k}'}}. \quad (7)$$

The critical temperature is then obtained in the standard way by taking the limit $T \rightarrow T_c$, $\Delta_n(k_z)$ close to zero in the above. More precisely, thanks to the matrix structure in the subband indices of the exchange integral, we get a linear system for the unknowns $\Delta_n(k_z)$, where we confine to $n = 1$ and $n = 2$. For $T = T_c$, the maximum eigenvalues of the matrix of the system is equal to 1 and this is the condition we seek when we solve for T_c . It is precisely this matrix structure which takes into account the interference between the electronic wave functions in the different subbands. The possibility of varying each matrix term allows us to study the superconducting phase when different condensates coexist in different coupling regimes and when it is possible to increase the critical temperature reaching high T_c superconductivity in the weak coupling regime with optimal choice of the nanoscale lattice parameters of particular metallic heterostructure at atomic limit [61,60,81,82].

To analyze the effect of increasing RSOC strength, we consider three cases with $\alpha_{SO} = 0.0, 0.4, 0.7$. For each of the three cases, we calculate T_c as a function of the Lifshitz parameter η at a fixed renormalized electron-phonon coupling g . The latter is given by $g = \gamma_0/(1 + \gamma_0)$ and is varied in the range $0 < g < 0.5$ for $0 < \gamma_0 < 1$, where $\gamma_0 = \Gamma/\omega_0$ has been obtained in Ref.[63] by measuring the width of the Raman line Γ , and the phonon energy ω_0 .

We have been inspired here by the data available for the archetypal case of natural layered two-gap superconductor, the doped MgB_2 [88] with chemical formula $Mg_{1-x}A_xB_2$ with $A = \text{Al}$ or Sc , where the $T_c(x)$ and $T_c(\eta)$ have been measured [62 and 83]. In the doped MgB_2 the first Fermi surface is made of boron π orbitals and the second appearing Fermi surface is made of quasi two-dimensional boron σ orbitals. The critical temperature T_c in $Mg_{1-x}Al_xB_2$ as a function of the Lifshitz parameter η is plotted in panel (a) of Fig. 2. In fact the Al(3+) dopants replace Mg(2+) ions in the spacer atomic layers and therefore tune the charge density in the boron layers via the charge transfer from the spacer layers to the superconducting boron layers (due the different charge in the Al dopant ion and Mg ion). Band structure calculations have been used to get the transverse hopping energy ΔE between boron σ two-dimensional orbitals [62 and 83] needed for the calculation of η . Al doping in $Mg_{1-x}Al_xB_2$ induces the variation of the electron-phonon coupling for the carriers in the appearing σ band which has been measured by Raman spectroscopy in Ref. [63]. Panel (b) of Fig. 2 shows the softening of the energy ω_0 of the E_{2g} phonon mode and the variation of the reduced electron-phonon coupling g as a function of η in in $Mg_{1-x}Al_xB_2$. In the case of $Mg_{1-x}Al_xB_2$ it is necessary to take into account the presence of nanoscale

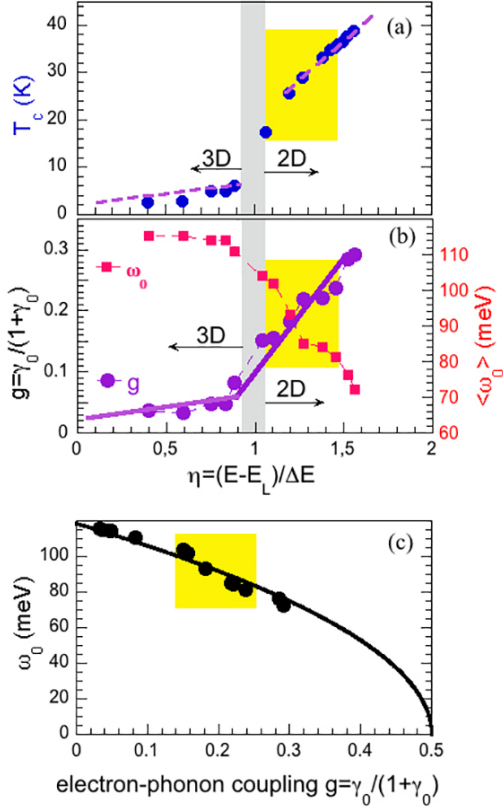


Figure 2. Panel (a) shows the superconducting critical temperature of $Mg_{1-x}Al_xB_2$ as a function of the Lifshitz parameter η where E_L is the energy of the chemical potential for the appearing of the σ Fermi surface and ΔE is the dispersion of the σ band in the transversal z direction [63]. Panel(b) shows the energy of the E_{2g} phonon-mode, ω_0 , in $Mg_{1-x}Al_xB_2$, measured by Raman spectroscopy [63] as a function of the Lifshitz parameter η . The yellow regions indicate the phase-separation regime near the 2D-3D Lifshitz topological transition observed experimentally [63, 83] predicted in Ref. [84–87]. Panel (c) shows the experimental data ω_0 as a function of g fitted with the Migdal relation, $\omega_0 = \tilde{\omega}_0 \sqrt{1 - 2g}$, where $\tilde{\omega}_0 = 120$ meV.

phase separation near the Lifshitz transition [89] which appears in the yellow area in Fig. 2, where the data indicate the averaged values of the two split Raman lines. In fact while for a non interacting Fermi gas the topological Lifshitz transitions are of 2.5 order, here for interacting particles in the appearing of a new Fermi surface the Lifshitz transition becomes a first order transition with phase separation [84–87] and critical opalescence [65, 90–93].

The panel (c) of Fig. 2 shows the experimental softening of the energy ω_0 of the E_{2g} phonon mode in $Mg_{1-x}Al_xB_2$ [63] as a function of the electron-phonon coupling g . The figure shows that the data can be fitted with the Migdal relation [94], between the renormalized cut-off energy, ω_0 , and g , where the bare cut-off energy

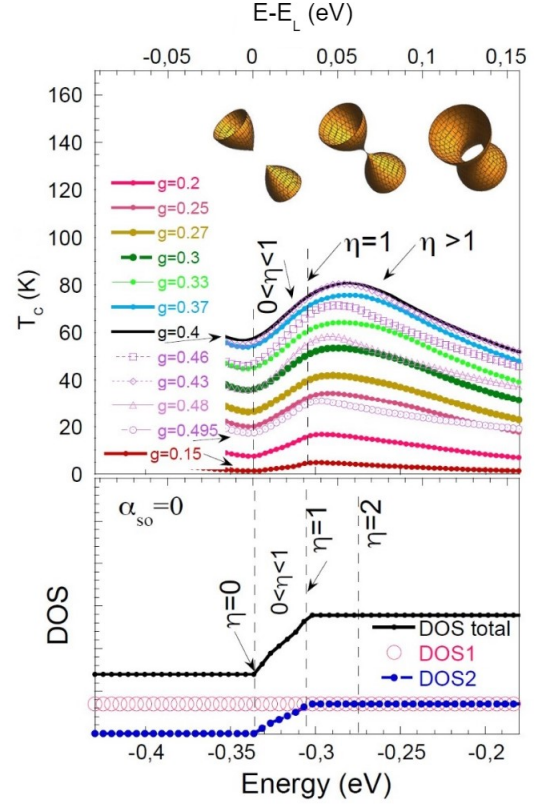


Figure 3. The superconducting critical temperature as function of the chemical potential measured relative to the top of the periodic potential barrier (taken as the zero energy) and the density of states, DOS, of the normal phase in lower panel of an artificial superlattice of quantum wells without RSOC i.e., $\alpha_{SO} = 0$. On the upper part of the figure we show the Fermi surface topology for three typical values of the Lifshitz parameter, $\eta \gtrless 1$ defined by the Eq.1. T_c is plotted as a function of the energy of the chemical potential for many values of the electron-phonon coupling g in the range $[0 : 0.5]$ where the energy cut-off is related to g following the Migdal relation (Eq.8) as in panel (c) of Fig. 2. The critical temperature reaches a maximum value equal to 80 K for $g = 0.4$. In the lower panel we plot the partial DOS for the first subband (pink dots) and for the second subband (blue dots) with the total DOS (black dots) as a function of the energy, showing the typical pattern of a superlattice of interacting layers.

is given by $\tilde{\omega}_0$:

$$\omega_0 = \tilde{\omega}_0 \sqrt{1 - 2g}. \quad (8)$$

This relation (8) shows that by tuning the chemical potential near the Kohn anomaly [83] the phonon energy approaches zero and the electron-phonon coupling approaches $g = 0.5$. The fitted Migdal relation between ω_0 and g is shown in panel (c) of Fig. 2 for the material design of nanoscale artificial superlattices of quantum wells.

Fig. 3 shows the calculated superconducting temperature T_c as a function of the chemical potential for the

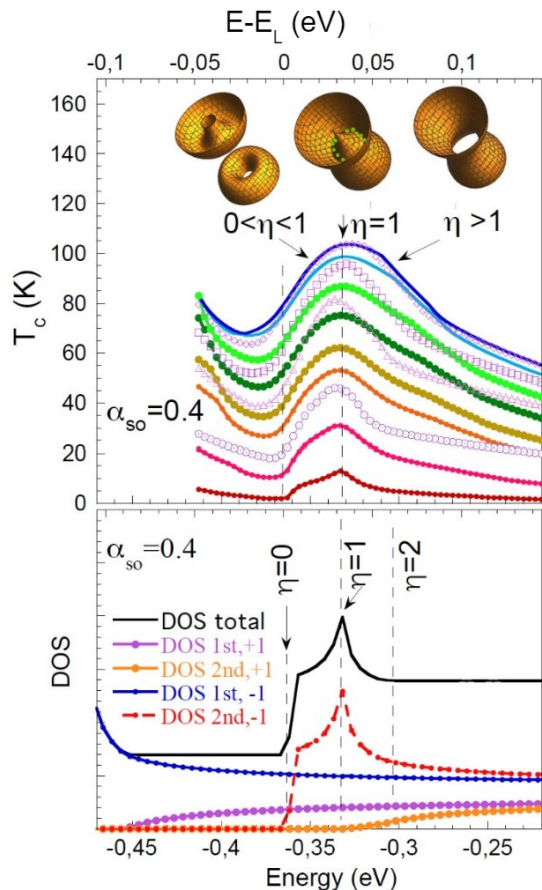


Figure 4. The superconducting critical temperature, panel (a), as function of the chemical potential measured relative to the top of the periodic potential barrier (taken as the zero energy level) and the density of states, DOS, panel (b), of the normal phase for an artificial superlattice of quantum wells with an internal electric field, giving a spin orbit coupling, $\alpha_{SO} = 0.4$. The Fermi surfaces for three values of the Lifshitz parameter, $\eta \gtrsim 1$ defined by the Eq.1 are shown in the upper part of the figure to show the topological Lifshitz transition of the appearing new Fermi surface from a torus to a corrugated cylinder for $\eta > 1$.

superlattice shown in Fig. 1 and the total and partial density of states, DOS, of the normal phase for $\alpha_{SO} = 0$. For $\alpha_{SO} = 0$ the total DOS shows the step-like behavior typical of the superlattice of quantum wells at the appearing of the 3D Fermi surface and the flat density DOS where the Fermi surface is a corrugated cylinder above the Lifshitz transition of the type opening a neck. The panel (a) of the Fig. 3 shows the critical temperature as a function of the chemical potential for different values of the electron-phonon coupling g and different phonon cut-off energy ω_0 , which are related by the phenomenological Migdal relation shown in panel (c) of Fig. 2. In the lower part of the Fig. 3 we report the partial DOS for the first two subbands and the total DOS of the superlattice. The critical temperature shows a dip when the chemical po-

tential is tuned at the band-edge of the second subband ($\eta = 0$), due to the negative interference effect typical of a Fano antiresonance between the two pairing channels. We observe at $\eta = 0$ a topological Lifshitz transition of the first type, with the appearing of a new closed 3D Fermi surface [28, 54, 57–59, 69, 88, 95, and 96]. At $\eta = 1$, we have a second Lifshitz transition of the second type, called *opening a neck*, where the Fermi surface changes the topology from 3D to a 2D corrugated cylinder. At this VHS there is only a singular point which is not enough to give a peak in the DOS, but it gives a peak in the critical temperature. For values of $\eta > 1$ the Fermi surface becomes a 2D corrugated cylinder. This figure shows that the maximum of the critical temperature due to the Fano-Feshbach resonance occurs where the Lifshitz parameter is in the range $\eta = 1.5$, i.e. well above the VHS associated to an isolated singularity. The results shows that in the absence of the RSOC it is possible to reach a maximum of the critical temperature of 80 K with a selected electron-phonon parameter $g = 0.4$, and about 40 K for $g = 0.3$ like in MgB_2 .

Fig. 4 shows the curves T_c versus the chemical potential in the presence of RSOC $\alpha_{SO} = 0.4$. The Fermi surfaces at three characteristic values of the Lifshitz parameter, for $\eta < 1$, at $\eta = 1$ and for $\eta > 1$ showing the topological Lifshitz transition in the upper part of the figure. In panel (a) of Fig. 4 we plot T_c as a function of the chemical potential for different values of the superconducting electron-phonon coupling g in the range $[0 : 0.5]$ where the energy cut-off is related to g following the Migdal relation (Eq.8) following the phenomenological relation shown in panel (c) of Fig. 2. The critical temperature increases with g for $g < 0.4$ where it reaches the maximum value $T_c = 120$ K. In panel (b) we plot the partial DOS for the first and for the second subband, for two values of the helicity and the total DOS (black dots) as a function of the energy. For positive helicity the DOS shows a trend very similar to that observed in the absence of RSOC. In the case of negative helicity we observe a sharp peak in the DOS which is linked to the unconventional Lifshitz transition of the Fermi surface topology from a torus to a corrugated cylinder.

For negative helicity, $\lambda = -1$, the DOS shows a peak where the Lifshitz parameter is equal to E_0/ω_0 , where $E_0 = -(m\alpha^2)/(2\hbar^2)$ is the Rashba energy shift. As it was shown in Ref.[61], the peak in the DOS is linked to an unusual variation in the topology of the Fermi surface (see the top panel in the Fig. 4). In particular, when the chemical potential reaches the second Lifshitz transition, an unconventional VHS is observed where the singular nodal points on the Fermi surface form an entire circle (highlighted with a green dashed curve), which explains the appearance of a peak in the DOS. The radius of the circle of singular points increases as the RSOC increases and this is associated with the shift of the DOS peak to lower energy (see Ref.[61]). The unconventional Lifshitz transition observed in the normal phase generates an amplification of the maximum critical temperature that goes

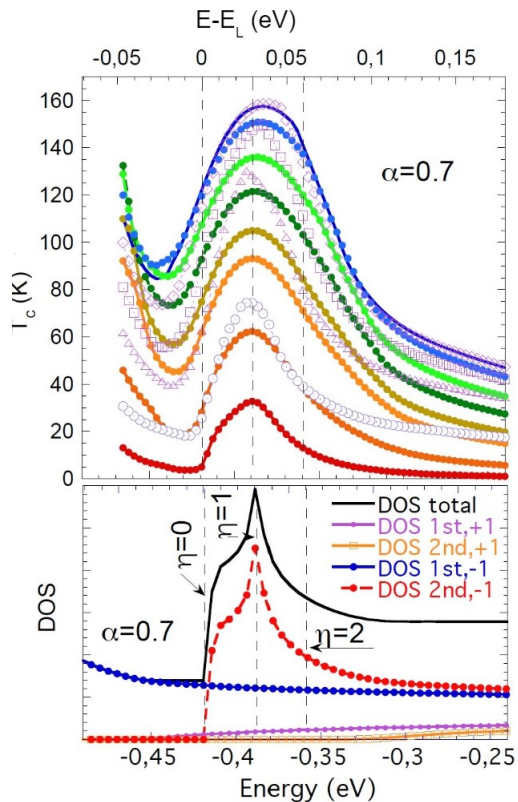


Figure 5. The superconducting critical temperature and the density of states, DOS, of the normal phase of an artificial superlattice of nanoscale layers (heterostructure of quantum layers) with RSOC, where $\alpha_{SO} = 0.7$, as a function of the chemical measured relative to the top of the potential barrier. Starting from the top we plot the Fermi surfaces for three values of the Lifshitz parameter, $\eta \gtrsim 1$, in the central panel we plot T_c as a function of the energy for different value of the superconducting coupling g in the range $[0 : 0.5]$, according to the Migdal relation (Eq.8). The critical temperature increases with g , reaches a maximum value equal to 160 K and goes toward zero at $g=0.5$. In the lower part of the figure we plot the partial DOS for the first and for the second subband, for two values of the helicity and the total DOS (black dots) as a function of the energy. This figure shows that by increasing the intensity of the RSOC, the peak of DOS increases and with it also the maximum critical temperature.

from 80 K, in the absence of RSOC, up to 120 K for $\alpha_{SO} = 0.4$. By further increasing the spin-orbit coupling up to $\alpha_{SO} = 0.7$, shown in Fig. 5, it is possible to reach at the top of the dome a critical temperature of 160 K, as in cuprate perovskite superconductors.

B. The superconducting dome

It is known that in the BCS theory for a single-gap superconductor the critical temperature depends on the renormalized electron-phonon coupling strength g , with

the phonon energy, ω_0 , playing the role of a pre-factor and of the energy cut-off of pairing interaction. Therefore in the BCS theories T_c it is not dependent on the variations of the chemical potential, since the Fermi level E_F is assumed to be far from band edges and much larger than the energy cut-off, $E_F/\omega_0 \gg 1$.

In two-gap superconductivity in artificial nanoscale superlattices near a topological Lifshitz transition the Fermi level in the new appearing second Fermi surface E_{F2} is near the band edge E_L (see the Eq.1) which is shifted in the presence of RSOC. Moreover the Fano resonance occurs where the Lifshitz parameter is tuned in the range $-1 < \eta < 3$ where $0 < (E_{F2} - E_L)/\omega_0 < 2$. Therefore in the two-gap superconductivity studied here the BPV theory allows to calculate the *superconducting dome* where the critical temperature depends on electron-phonon coupling g and the Lifshitz parameter η . Here we report the *superconducting dome* where T_c is a function of either the Lifshitz parameter η or the electron-phonon coupling g . The *superconducting dome* characterizes the superconducting properties of the artificial nanoscale superlattice with a given architecture needed for material design of novel artificial high- T_c superconductors.

Using the numerical results presented in the previous subsection we show in Fig. 6 the *superconducting domes* as colour plots of the critical temperature T_c as a function of the electron-phonon coupling g and the Lifshitz parameter η for three different values of spin orbit interaction RSOC $\alpha = 0, 0.4, 0.7$. The *superconducting domes* in Fig. 6 clearly shows that the maximum of the critical temperature is reached when the chemical potential is tuned at the unconventional topological Lifshitz transition of the type *opening a neck* near $\eta=1$, where the Fermi surface topology of the second subband changes from a closed 3D surface to a corrugated cylinder for $\alpha = 0$ and from a torus to a corrugated cylinder for $\alpha = 0.4, 0.7$ with a circle of singularity points giving a peak in the DOS. The top of the *superconducting dome* of the critical temperature increases with RSOC going to 90 K and 170 K as the spin-orbit coupling increases from zero to 0.4 and 0.7 respectively.

Empirical 3D phase diagrams, showing *superconducting domes* have been measured for high T_c superconductors, beyond the standard 2D phase diagram (T_c versus *doping*) introducing a second material dependent physical variable to explain experimental data of high T_c superconductivity. The third axis has been proposed to be the lattice strain [64 and 66], or electron-phonon interaction [65 and 67]. The difficulty in the interpretation of empirical 3D phase diagrams of high temperature superconductors from experimental data is due to the fact that in the experiments the variation of T_c is measured for changes of chemical doping, or external pressure or strain (micro-strain, misfit-strain) or gate-voltage which induce a joint variation of the chemical potential and electron-phonon coupling. Therefore the interpretation of the experimental curves of T_c versus η requires the knowledge of the response of T_c along a particular path-

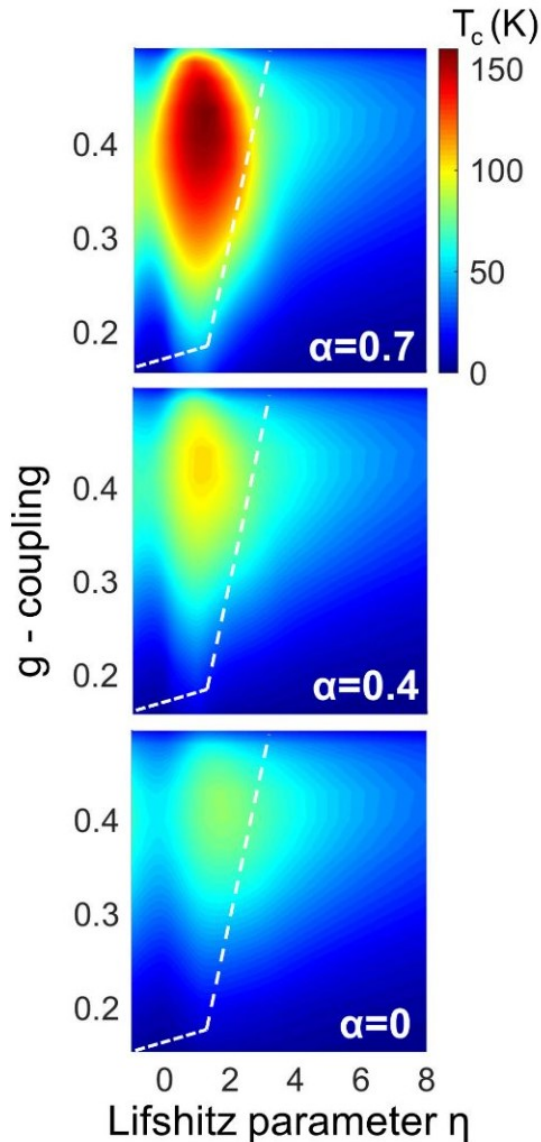


Figure 6. The three *superconducting domes* for artificial superlattices of quantum wells for three different values of the Rashba coupling constant $\alpha_{SO} = 0, 0.4, 0.7$. The colour plots show the superconducting critical temperature as a function of the Lifshitz parameter η measuring the position of the Fermi level E_{F2} and of the electron-phonon coupling g in the second subband. The critical temperature increases with the colour going from blue to red. The top of *superconducting dome* occurs near $g = 0.4$ and η about 1. We observe a shift of the top of the *superconducting dome* to lower η values from $\eta=1.5$ to $\eta=1$ increasing the spin-orbit coupling. The observed marked anisotropy of the superconducting dome is due to anisotropic line-shape of the Fano resonance. The white dashed line indicates the pathway in the (g, η) plane extracted from the experimental data for $Mg_{1-x}Al_xB_2$ shown in panel (b) of Fig. 2. In this pathway for $\eta < 1$ the electron-phonon coupling g is nearly constant around 0.1 and 0.15 while it shows a sharp change for $1 < \eta < 2.5$ with a rapid increase due to a Kohnanomaly.

way in the (η, g) plane.

The *superconducting dome* for artificial superlattice of quantum layers shown in Fig. 6 has been obtained using the phenomenological Migdal relation shown in panel (c) of Fig. 2 by fitting experimental data of doped MgB_2 . Therefore we can use the phenomenological pathway in the plane (η, g) shown in panel (b) of Fig. 2, which is indicated by the white dashed line in Fig. 6 to establish the theoretical prediction of the curve $T_c(\eta)$ for Al doping in $Mg_{1-x}Al_xB_2$. The pathway of g versus η in Fig. 6 shows low values of g with a nearly flat slope for $0 < \eta < 1$, where the second Fermi surface has a closed 3D shape and a very sharp change at the slope at $\eta = 1$, with g rapidly increasing in the range $1 < \eta < 3$, where the second Fermi surface is a corrugated cylinder.

In Fig. 7 we report the variation of the critical temperature T_c versus η where the superlattice of quantum wells is manipulated by doping, strain, pressure, or gate-voltage following the particular pathways in the (η, g) plane shown by the dashed line in Fig. 6. The predicted $T_c(\eta)$ curve for this particular pathway shown of Fig. 7 for $\alpha = 0$ is compared with the experimental curve of T_c versus η extracted from data on $Mg_{1-x}Al_xB_2$ in Ref.[63] shown in panel (a) of Fig. 2). The theory is able to reproduce the experimental data up to $T_{c,MAX} = 40$ K where $\eta = 1.5$ and $g = 0.3$

III. CONCLUSIONS

Here we have reported the calculation of the 2D superconducting dome for a 3 nm superlattice of quantum wells with Rashba spin orbit coupling. The Rashba coupling induces an unconventional Lifshitz transition associated with a VHS extended on a circumference of increasing radius with the intensity RSOC in negative helicity states [61]. The complexity in the properties of the normal phase is associated with a larger amplification of the gap and T_c . In particular, we have seen that the amplification increases when the chemical potential is varied around an unconventional Lifshitz transition. In this situation, in addition to the intra-band Cooper pairing, it is necessary to include the key role played by the quantum configuration interaction that appears in the mean-field equation for the self-consistency of the gap and which has to be calculated considering the exchange interactions between pairs of singlets in subbands with different quantum numbers and different helicities. The results show that T_c at the top of the *superconducting dome* increases up to 170K by increasing spin orbit coupling. The Rashba spin orbit coupling can be tuned by manipulation of ferroelectricity in the artificial superlattices. In fact, while it is known that 3D homogeneous metals cannot exhibit ferroelectricity because static internal electric fields are screened by conduction electrons, the coexistence of ferroelectricity and superconductivity is possible in inhomogeneous phases like our artificial superlattices of quantum wells if the insulating interca-

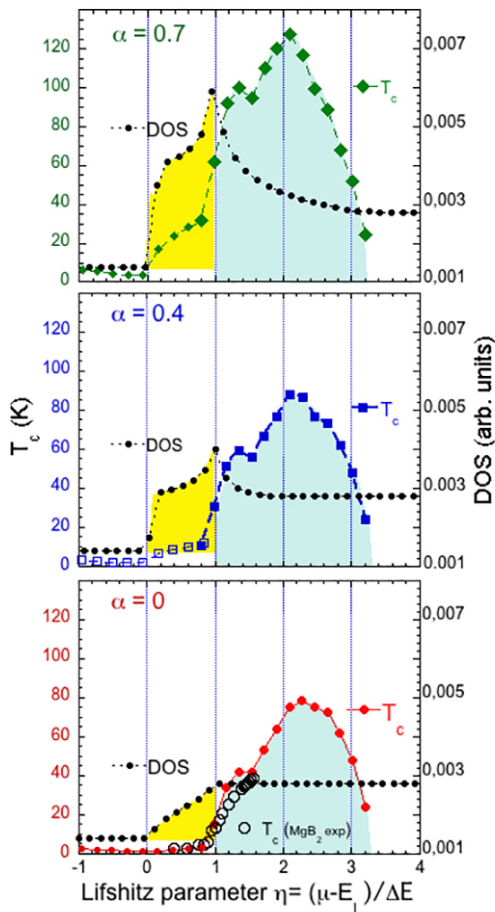


Figure 7. The critical temperature T_c versus η for the 3 nm artificial superlattice of quantum wells as a function of the particular pathway in the (η, g) plane indicated by the dashed line in Fig. 6 where the three panels show three different cases of spin orbit interaction RSOC $\alpha = 0, 0.4, 0.7$. The calculation for the case $\alpha = 0$ is compared with experimental data (open circles) measured in archetypal case of two-gap superconductivity in multi-layers $Mg_{1-x}Al_xB_2$ [63] tuned in the range of the Lifshitz transition for *opening a neck*. The variation of the density of states DOS along the same pathway is plotted to show that, in the scenario presented here, the variation of the superconducting critical temperature and the variation of the DOS do not show a trivial correlation.

lated layers show ferroelectricity. In fact the coexistence of ferroelectricity and the metallic phase has been observed in proximity to (i) phase separation at structural phase transitions [97], (ii) in metallic $LiOSO_3$ that is structurally equivalent to the ferroelectric transition of $LiNbO_3$ [98] and the coexistence is favored by electronic correlation and phase separation near metal-insulator transitions [99–101]. In the last ten years ferroelectricity and superconductivity have been observed in several metallic perovskites [98, 102–107] and a tunable spin-orbit coupling has been observed in nanoscale heterogeneous phases of matter [106, 108–112]. We have identified the particular pathway in the (η, g) plane of the su-



Figure 8. Prof. Yvette Cauchois at Solvay Conference 1951, she is the third in the first row. The Picture is by G. Coopmans <http://www.hilliontchernobyl.com/solvay1951.htm>.

perconducting dome $T_c(\eta, g)$ from experimental Raman data giving $g(\eta)$ for the natural superlattice of superconducting boron atomic layers in $Mg_{1-x}Al_xB_2$ intercalated by normal Al-Mg layers. In this experimental pathway the intra-band electron-phonon coupling is weak near the band edge in the appearing small 3D Fermi surface and it shows a rapid increase in the corrugated 2D cylindrical Fermi surface where it crosses a Kohn anomaly approaching the maximum T_c . Moreover we have added the spin degree of freedom to be able to take into account the RSOC coupling, hence we have solved the Dirac equation in non-relativistic limit to determine the correct shape of the wave-functions needed for the calculation of energy dependent pair transfer exchange interaction. Therefore this work provides the quantum scenario of two-gap superconductivity near an unconventional Lifshitz transition associated with a VHS extended on a circumference in the negative helicity states, whose radius increases as the RSOC increases. Moreover here we overcome the previous theoretical approaches where the adiabatic limit was considered i.e., where the Fermi energy is much larger than the Rashba shift and the gap energy, while the interesting physics occur in a regime where the Fermi energy in the second subband is of the same order of magnitude as the pairing energy and the spin-orbit splitting induced by the RSOC. Finally we have shown that by design of the heterostructure nanoscale geometry, and the choice of different materials for metallic layers and spacer layers, it is possible to amplify the critical temperature by using the joint effect of the Fano resonance between the superconducting gaps, the electron-phonon interaction near a Kohn anomaly in a corrugated cylinder Fermi surface and the RSOC in nanoscale superlattices of quantum wells.

IV. DEDICATION

This paper is dedicated to Yvette Cauchois (1908-1999) [113], Fig. 8, a pioneer of X-ray spectroscopy [43] and its applications to identify localised versus delocalised electronic states in condensed matter giving white lines or absorption edges respectively [114] which later have allowed the experimental identification of two-band, two-gap superconductors. She collaborated with Ugo Fano [115] and she made the first experiment on applied physics using synchrotron radiation in Europe [116].

ACKNOWLEDGMENTS

We acknowledge financial support of Superstripes on-lus.

-
- [1] R. Dingle, W. Wiegmann, and C. Henry, Quantum states of confined carriers in very thin $\text{Al}_x\text{Ga}_{1-x}\text{As-GaAs-Al}_x\text{Ga}_{1-x}\text{As}$ heterostructures, *Phys. Rev. Lett.* **33**, 827 (1974).
- [2] A. J. Nozik, Quantization effects in semiconductor nanostructures and singlet fission in molecular chromophores for photovoltaics and solar fuels, *Chemical Physics Reviews* **2**, 021305 (2021).
- [3] D. A. Bandurin, A. V. Tyurnina, G. L. Yu, A. Mishchenko, V. Zólyomi, S. V. Morozov, R. K. Kumar, R. V. Gorbachev, Z. R. Kudrynskiy, S. Pezzini, *et al.*, High electron mobility, quantum hall effect and anomalous optical response in atomically thin InSe, *Nature nanotechnology* **12**, 223 (2017).
- [4] G. Mudd, S. Svatek, L. Hague, O. Makarovskiy, Z. Kudrynskiy, C. Mellor, P. Beton, L. Eaves, K. Novoselov, Z. Kovalyuk, *et al.*, High broad-band photoresponsivity of mechanically formed in-se-graphene van der Waals heterostructures, *Advanced Materials* **27**, 3760 (2015).
- [5] L. Li, G. Ye, V. Tran, R. Fei, G. Chen, H. Wang, J. Wang, K. Watanabe, T. Taniguchi, L. Yang, *et al.*, Quantum oscillations in a two-dimensional electron gas in black phosphorus thin films, *Nature nanotechnology* **10**, 608 (2015).
- [6] K. F. Mak, C. Lee, J. Hone, J. Shan, and T. F. Heinz, Atomically thin MoS_2 : a new direct-gap semiconductor, *Phys. Rev. Lett.* **105**, 136805 (2010).
- [7] F. Baiutti, G. Christiani, and G. Logvenov, Towards precise defect control in layered oxide structures by using oxide molecular beam epitaxy, *Beilstein Journal of Nanotechnology* **5**, 596 (2014).
- [8] Y. Suyolcu, G. Christiani, P. van Aken, and G. Logvenov, Design of complex oxide interfaces by oxide molecular beam epitaxy, *Journal of Superconductivity and Novel Magnetism* **33**, 107 (2020).
- [9] A. Bianconi, High T_c superconductors made by metal heterostructures at the atomic limit, *European Patent EP0733271* Sept **25** (1996).
- [10] A. Bianconi, Process of increasing the critical temperature T_c of a bulk superconductor by making metal heterostructures at the atomic limit, *US Patent 6,265,019* (2001).
- [11] D. Innocenti, N. Poccia, A. Ricci, A. Valletta, S. Caprara, A. Perali, and A. Bianconi, Resonant and crossover phenomena in a multiband superconductor: Tuning the chemical potential near a band edge, *Physical Review B* **82**, 184528 (2010).
- [12] D. Innocenti, S. Caprara, N. Poccia, A. Ricci, A. Valletta, and A. Bianconi, Shape resonance for the anisotropic superconducting gaps near a Lifshitz transition: the effect of electron hopping between layers, *Superconductor Science and Technology* **24**, 015012 (2010).
- [13] A. Bianconi, D. Innocenti, A. Valletta, and A. Perali, Shape resonances in superconducting gaps in a 2deg at oxide-oxide interface, in *Journal of Physics: Conference Series*, Vol. 529 (IOP Publishing, 2014) p. 012007.
- [14] V. Moskalenko, Superconductivity in metals with overlapping energy bands, *Fiz. Metal. Metalloved* **8**, 2518 (1959).
- [15] H. Suhl, B. Matthias, and L. Walker, Bardeen-cooper-schrieffer theory of superconductivity in the case of overlapping bands, *Physical Review Letters* **3**, 552 (1959).
- [16] G. Ummarino, R. Gonnelli, S. Massidda, and A. Bianconi, Two-band Eliashberg equations and the experimental T_c of the diboride $\text{Mg}_{1-x}\text{Al}_x\text{B}_2$, *Physica C: Superconductivity* **407**, 121 (2004).
- [17] A. Bussmann-Holder and A. Bianconi, Raising the diboride superconductor transition temperature using quantum interference effects, *Phys. Rev. B* **67**, 132509 (2003).
- [18] R. Friedberg and T. D. Lee, Gap energy and long-range order in the boson-fermion model of superconductivity, *Physical Review B* **40**, 6745 (1989).
- [19] F. Palumbo, A. Marcelli, and A. Bianconi, From the pion cloud of Tomonaga to the electron pairs of Schrieffer: many body wave functions from nuclear physics to condensed matter physics, *Journal of Superconductivity and Novel Magnetism* **29**, 3107 (2016).
- [20] T. Geballe and B. Y. Mozyzhes, Qualitative understanding of the highest T_c cuprates, *Physica C: Superconductivity* **341**, 1821 (2000).
- [21] A. Menushenkov, A. Kuznetsov, K. Klementiev, and M. Y. Kagan, Fermi-Bose mixture in $\text{Ba}(\text{K})\text{BiO}_3$ superconducting oxide, *Journal of Superconductivity and Novel Magnetism* **29**, 701 (2016).
- [22] M. Dzero and J. Schmalian, Superconductivity in charge Kondo systems, *Physical Review Letters* **94**, 157003 (2005).
- [23] A. Bianconi, A. Valletta, A. Perali, and N. L. Saini, Superconductivity of a striped phase at the atomic limit, *Physica C: Superconductivity* **296**, 269 (1998).
- [24] A. Perali, A. Bianconi, A. Lanzara, and N. L. Saini, The gap amplification at a shape resonance in a superlattice of quantum stripes: A mechanism for high T_c , *Solid State Communications* **100**, 181 (1996).
- [25] A. Valletta, A. Bianconi, A. Perali, and N. Saini, Electronic and superconducting properties of a superlattice of quantum stripes at the atomic limit, *Zeitschrift für Physik B Condensed Matter* **104**, 707 (1997).
- [26] A. Perali, P. Pieri, L. Pisani, and G. Strinati, BCS-BEC crossover at finite temperature for superfluid trapped fermi atoms, *Physical Review Letters* **92**, 220404 (2004).
- [27] A. Perali, P. Pieri, and G. Strinati, Quantitative comparison between theoretical predictions and experimental results for the BCS-BEC crossover, *Physical Review Letters* **93**, 100404 (2004).

- [28] A. Perali, D. Innocenti, A. Valletta, and A. Bianconi, Anomalous isotope effect near a 2.5 Lifshitz transition in a multi-band multi-condensate superconductor made of a superlattice of stripes, *Superconductor Science and Technology* **25**, 124002 (2012).
- [29] A. Shanenko, M. D. Croitoru, A. Vagov, V. M. Axt, A. Perali, and F. Peeters, Atypical BCS-BEC crossover induced by quantum-size effects, *Physical Review A* **86**, 033612 (2012).
- [30] Y. Chen, A. Shanenko, A. Perali, and F. Peeters, Superconducting nanofilms: molecule-like pairing induced by quantum confinement, *Journal of Physics: Condensed Matter* **24**, 185701 (2012).
- [31] M. Cariglia, A. Vargas-Paredes, M. M. Doria, A. Bianconi, M. V. Milošević, and A. Perali, Shape-resonant superconductivity in nanofilms: from weak to strong coupling, *Journal of Superconductivity and Novel Magnetism* **29**, 3081 (2016).
- [32] A. Guidini and A. Perali, Band-edge BCS-BEC crossover in a two-band superconductor: physical properties and detection parameters, *Superconductor Science and Technology* **27**, 124002 (2014).
- [33] A. Guidini, L. Flammia, M. V. Milošević, and A. Perali, BCS-BEC crossover in quantum confined superconductors, *Journal of Superconductivity and Novel Magnetism* **29**, 711 (2016).
- [34] M. M. Doria, M. Cariglia, and A. Perali, Multigap superconductivity and barrier-driven resonances in superconducting nanofilms with an inner potential barrier, *Physical Review B* **94**, 224513 (2016).
- [35] L. Salasnich, A. Shanenko, A. Vagov, J. A. Aguiar, and A. Perali, Screening of pair fluctuations in superconductors with coupled shallow and deep bands: A route to higher-temperature superconductivity, *Physical Review B* **100**, 064510 (2019).
- [36] A. Shanenko, M. Croitoru, M. Zgirski, F. Peeters, and K. Arutyunov, Size-dependent enhancement of superconductivity in Al and Sn nanowires: Shape-resonance effect, *Physical Review B* **74**, 052502 (2006).
- [37] D. Valentinis, D. Van Der Marel, and C. Berthod, BCS superconductivity near the band edge: Exact results for one and several bands, *Physical Review B* **94**, 024511 (2016).
- [38] Tajima, H. and A. Perali, and P. Pieri, BCS-BEC crossover and pairing fluctuations in a two band superfluid/superconductor: A T matrix approach, *Condensed Matter* **5**, 10 (2020).
- [39] A. Vargas-Paredes, A. Shanenko, A. Vagov, M. Milošević, and A. Perali, Crossband versus intraband pairing in superconductors: Signatures and consequences of the interplay, *Physical Review B* **101**, 094516 (2020).
- [40] K. Ochi, H. Tajima, K. Iida, and H. Aoki, Resonant pair-exchange scattering and BCS-BEC crossover in a system composed of dispersive and heavy incipient bands: A feshbach analogy, *Physical Review Research* **4**, 013032 (2022).
- [41] M. Y. Kagan and A. Bianconi, Fermi-Bose mixtures and BCS-BEC crossover in high- T_c superconductors, *Condensed Matter* **4**, 51 (2019).
- [42] U. Fano, Effects of configuration interaction on intensities and phase shifts, *Physical Review* **124**, 1866 (1961).
- [43] Y. Cauchois, La spectroscopie X, *Zeitschrift für Kristallographie-Crystalline Materials* **120**, 182 (1964).
- [44] U. Fano and J. Cooper, Spectral distribution of atomic oscillator strengths, *Reviews of Modern Physics* **40**, 441 (1968).
- [45] A. Bianconi, S. Della Longa, C. Li, M. Pompa, A. Congiu-Castellano, D. Udron, A. Flank, and P. Lagarde, Linearly polarized Cu L_3 -edge X-ray-absorption near-edge structure of $\text{Bi}_2\text{CaSr}_2\text{Cu}_2\text{O}_8$, *Physical Review B* **44**, 10126 (1991).
- [46] B. Luk'Yanchuk, N. I. Zheludev, S. A. Maier, N. J. Halas, P. Nordlander, H. Giessen, and C. T. Chong, The Fano resonance in plasmonic nanostructures and metamaterials, *Nature materials* **9**, 707 (2010).
- [47] A. E. Miroshnichenko, S. Flach, and Y. S. Kivshar, Fano resonances in nanoscale structures, *Reviews of Modern Physics* **82**, 2257 (2010).
- [48] M. F. Limonov, Fano resonance for applications, *Advances in Optics and Photonics* **13**, 703 (2021).
- [49] H. Feshbach, A unified theory of nuclear reactions. II, *Annals of Physics* **19**, 287 (1962).
- [50] M. Zwerlein, C. Stan, C. Schunck, S. Raupach, A. Kerman, and W. Ketterle, Condensation of pairs of fermionic atoms near a Feshbach resonance, *Physical Review Letters* **92**, 120403 (2004).
- [51] A. Vittorini-Orgeas and A. Bianconi, From Majorana theory of atomic autoionization to Feshbach resonances in high temperature superconductors, *Journal of Superconductivity and Novel Magnetism* **22**, 215 (2009).
- [52] B. N. Bogoliubov, V. Tolmachev, and D. Shirkov, A new method in the theory of superconductivity, *Soviet Physics JETP* **34**, 1 (1958).
- [53] B. V. Svistunov, E. S. Babaev, and N. V. Prokof'ev, *Superfluid states of matter* (Crc Press, 2015).
- [54] D. Innocenti and A. Bianconi, Isotope effect at the Fano resonance in superconducting gaps for multiband superconductors at a 2.5 Lifshitz transition, *Journal of Superconductivity and Novel Magnetism* **26**, 1319 (2013).
- [55] A. Bianconi, Shape resonances in multi-condensate granular superconductors formed by networks of nanoscale-stripped puddles, *Journal of Physics: Conference Series* **449**, 012002 (2013).
- [56] A. Bianconi and T. Jarlborg, Lifshitz transitions and zero point lattice fluctuations in sulfur hydride showing near room temperature superconductivity, *Novel Superconducting Materials* **1**, 37 (2015).
- [57] A. Bianconi and T. Jarlborg, Superconductivity above the lowest earth temperature in pressurized sulfur hydride, *EPL (Europhysics Letters)* **112**, 37001 (2015).
- [58] A. Bianconi, Superconductivity in quantum complex matter: the superstripes landscape, *Journal of Superconductivity and Novel Magnetism* **33**, 2269 (2020).
- [59] A. Valletta, G. Bardelloni, M. Brunelli, A. Lanzara, A. Bianconi, and N. Saini, T_c amplification and pseudo-gap at a shape resonance in a superlattice of quantum stripes, *Journal of Superconductivity* **10**, 383 (1997).
- [60] M. V. Mazziotti, A. Valletta, G. Campi, D. Innocenti, A. Perali, and A. Bianconi, Possible fano resonance for high- t_c multi-gap superconductivity in p-terphenyl doped by K at the Lifshitz transition, *EPL (Europhysics Letters)* **118**, 37003 (2017).
- [61] M. V. Mazziotti, A. Valletta, R. Raimondi, and A. Bianconi, Multigap superconductivity at an unconventional Lifshitz transition in a three-dimensional rashba heterostructure at the atomic limit, *Phys. Rev. B* **103**, 024523 (2021).

- [62] D. Di Castro, S. Agrestini, G. Campi, A. Cassetta, M. Colapietro, A. Congeduti, A. Continenza, S. De Negri, M. Giovannini, S. Massidda, *et al.*, The amplification of the superconducting t_c by combined effect of tuning of the Fermi level and the tensile micro-strain in $\text{Al}_{1-x}\text{Mg}_x\text{B}_2$, *EPL (Europhysics Letters)* **58**, 278 (2002).
- [63] L. Simonelli, V. Palmisano, M. Fratini, M. Filippi, P. Parisiades, D. Lampakis, E. Liarokapis, and A. Bianconi, Isotope effect on the E_2g phonon and mesoscopic phase separation near the electronic topological transition in $\text{Mg}_{1-x}\text{Al}_x\text{B}_2$, *Physical Review B* **80**, 014520 (2009).
- [64] S. Agrestini, D. Di Castro, M. Sansone, N. Saini, A. Saccone, S. De Negri, M. Giovannini, M. Colapietro, and A. Bianconi, High T_c superconductivity in a critical range of micro-strain and charge density in diborides, *Journal of Physics: Condensed Matter* **13**, 11689 (2001).
- [65] A. Bianconi, S. Agrestini, G. Bianconi, D. Di Castro, and N. Saini, A quantum phase transition driven by the electron lattice interaction gives high T_c superconductivity, *Journal of alloys and compounds* **317**, 537 (2001).
- [66] S. Agrestini, N. Saini, G. Bianconi, and A. Bianconi, The strain of CuO_2 lattice: the second variable for the phase diagram of cuprate perovskites, *Journal of Physics A: Mathematical and General* **36**, 9133 (2003).
- [67] Y. He, M. Hashimoto, D. Song, S.-D. Chen, J. He, I. Vishik, B. Moritz, D.-H. Lee, N. Nagaosa, J. Zaanen, *et al.*, Rapid change of superconductivity and electron-phonon coupling through critical doping in Bi-2212 , *Science* **362**, 62 (2018).
- [68] L. P. Gor'kov and E. I. Rashba, Superconducting 2D system with lifted spin degeneracy: mixed singlet-triplet state, *Physical Review Letters* **87**, 037004 (2001).
- [69] A. Bianconi, Feshbach shape resonance in multiband superconductivity in heterostructures, *Journal of Superconductivity* **18**, 625 (2005).
- [70] T. Jarlborg and A. Bianconi, Breakdown of the Migdal approximation at Lifshitz transitions with giant zero-point motion in the H_3S superconductor, *Scientific Reports* **6**, 24816 (2016).
- [71] A. Perali, A. Valletta, G. Bardeiloni, A. Bianconi, A. Lanzara, and N. Saini, The isotope effect in a superlattice of quantum stripes, *Journal of Superconductivity* **10**, 355 (1997).
- [72] E. I. Rashba, Properties of semiconductors with an extremum loop. I. cyclotron and combinational resonance in a magnetic field perpendicular to the plane of the loop, *Soviet Physics, Solid State* **2**, 1109 (1960).
- [73] E. Cappelluti, C. Grimaldi, and F. Marsiglio, Topological change of the Fermi surface in low-density Rashba gases: application to superconductivity, *Physical Review Letters* **98**, 167002 (2007).
- [74] S. Caprara, F. Peronaci, and M. Grilli, Intrinsic instability of electronic interfaces with strong Rashba coupling, *Physical Review Letters* **109**, 196401 (2012).
- [75] S. Caprara, D. Bucheli, M. Grilli, J. Biscaras, N. Bergeal, S. Hurand, C. Feuillet-Palma, J. Lesueur, A. Rastogi, and R. Budhani, Inhomogeneous electron gas at oxide interfaces with strong Rashba spin-orbit coupling, in *Spin*, Vol. 4 (World Scientific, 2014) p. 1440004.
- [76] V. Brosco and C. Grimaldi, Anisotropy of transport in bulk Rashba metals, *Physical Review B* **95**, 195164 (2017).
- [77] M. V. Mazziotti, N. Scopigno, M. Grilli, and S. Caprara, Majorana fermions in one-dimensional structures at $\text{LaAlO}_3/\text{SrTiO}_3$ oxide interfaces, *Condensed Matter* **3**, 37 (2018).
- [78] G. Volovik and K. Zhang, Lifshitz transitions, type-ii Dirac and Weyl fermions, event horizon and all that, *Journal of Low Temperature Physics* **189**, 276 (2017).
- [79] G. Volovik, Topological Lifshitz transitions, *Low Temperature Physics* **43**, 47 (2017).
- [80] G. E. Volovik, Exotic lifshitz transitions in topological materials, *Physics-Uspekhi* **61**, 89 (2018).
- [81] M. V. Mazziotti, R. Raimondi, A. Valletta, G. Campi, and A. Bianconi, Resonant multi-gap superconductivity at room temperature near a Lifshitz topological transition in sulfur hydrides, *Journal of Applied Physics* **130**, 173904 (2021).
- [82] M. V. Mazziotti, T. Jarlborg, A. Bianconi, and A. Valletta, Room temperature superconductivity dome at a Fano resonance in superlattices of wires, *Europhysics Letters* **134**, 17001 (2021).
- [83] S. Agrestini, C. Metallo, M. Filippi, L. Simonelli, G. Campi, C. Sanipoli, E. Liarokapis, S. De Negri, M. Giovannini, A. Saccone, *et al.*, Substitution of Sc for Mg in MgB_2 : Effects on transition temperature and Kohn anomaly, *Physical Review B* **70**, 134514 (2004).
- [84] K. Kugel, A. Rakhmanov, and A. Sboychakov, Phase separation in Jahn-Teller systems with localized and itinerant electrons, *Physical Review Letters* **95**, 267210 (2005).
- [85] K. Kugel, A. Rakhmanov, A. Sboychakov, F. Kusmartsev, N. Poccia, and A. Bianconi, A two-band model for the phase separation induced by the chemical mismatch pressure in different cuprate superconductors, *Superconductor Science and Technology* **22**, 014007 (2008).
- [86] A. Bianconi, N. Poccia, A. Sboychakov, A. Rakhmanov, and K. Kugel, Intrinsic arrested nanoscale phase separation near a topological Lifshitz transition in strongly correlated two-band metals, *Superconductor Science and Technology* **28**, 024005 (2015).
- [87] K. Kugel, A. Rakhmanov, A. Sboychakov, N. Poccia, and A. Bianconi, Model for phase separation controlled by doping and the internal chemical pressure in different cuprate superconductors, *Physical Review B* **78**, 165124 (2008).
- [88] A. Bianconi, D. Di Castro, S. Agrestini, G. Campi, N. Saini, A. Saccone, S. De Negri, and M. Giovannini, A superconductor made by a metal heterostructure at the atomic limit tuned at the shape resonance: MgB_2 , *Journal of Physics: Condensed Matter* **13**, 7383 (2001).
- [89] V. Palmisano, L. Simonelli, A. Puri, M. Fratini, Y. Busby, P. Parisiades, E. Liarokapis, M. Brunelli, A. Fitch, and A. Bianconi, Controlling mesoscopic phase separation near electronic topological transitions via quenched disorder in ternary diborides, *Journal of Physics: Condensed Matter* **20**, 434222 (2008).
- [90] A. Bianconi, G. Bianconi, S. Caprara, D. Di Castro, H. Oyanagi, and N. Saini, The stripe critical point for cuprates, *Journal of Physics: Condensed Matter* **12**, 10655 (2000).
- [91] T. Yamaji, Youhei Misawa and M. Imada, Condensed matter: Electronic structure and electrical, magnetic, and optical properties-quantum and topological criticalities of Lifshitz transition in two-dimensional corre-

- lated electron systems, Journal of the Physical Society of Japan **75**, 94719 (2006).
- [92] T. Misawa, Y. Yamaji, and M. Imada, Quantum critical opalescence around metal-insulator transitions, Journal of the Physical Society of Japan **75**, 083705 (2006).
- [93] Y. Yamaji, T. Misawa, and M. Imada, Quantum criticalities induced by Lifshitz transitions, Journal of magnetism and magnetic materials **310**, 838 (2007).
- [94] A. Migdal, Interaction between electrons and lattice vibrations in a normal metal, Sov. Phys. JETP **7**, 996 (1958).
- [95] A. Bianconi, On the Fermi liquid coupled with a generalized Wigner polaronic CDW giving high T_c superconductivity, Solid State Communications **91**, 1 (1994).
- [96] A. Bianconi, N. Saini, S. Agrestini, D. D. Castro, and G. Bianconi, The strain quantum critical point for superstripes in the phase diagram of all cuprate perovskites, International Journal of Modern Physics B **14**, 3342 (2000).
- [97] L. Testardi, Structural instability and superconductivity in A-15 compounds, Reviews of Modern Physics **47**, 637 (1975).
- [98] H. Boysen and F. Altorfer, A neutron powder investigation of the high-temperature structure and phase transition in LiNbO_3 , Acta Crystallographica Section B: Structural Science **50**, 405 (1994).
- [99] T. Egami, S. Ishihara, and M. Tachiki, Lattice effect of strong electron correlation: Implication for ferroelectricity and superconductivity, Science **261**, 1307 (1993).
- [100] A. Bianconi, Multiplet splitting of final-state configurations in X-ray-absorption spectrum of metal VO_2 : Effect of core-hole-screening, electron correlation, and metal-insulator transition, Physical Review B **26**, 2741 (1982).
- [101] G. Bianconi, Superconductor-insulator transition on annealed complex networks, Physical Review E **85**, 061113 (2012).
- [102] T. Kolodiazny, M. Tachibana, H. Kawaji, J. Hwang, and E. Takayama-Muromachi, Persistence of ferroelectricity in BaTiO_3 through the insulator-metal transition, Physical Review Letters **104**, 147602 (2010).
- [103] Y. Shi, Y. Guo, X. Wang, A. J. Princep, D. Khalyavin, P. Manuel, Y. Michiue, A. Sato, K. Tsuda, S. Yu, *et al.*, A ferroelectric-like structural transition in a metal, Nature Materials **12**, 1024 (2013).
- [104] R. Russell, N. Ratcliff, K. Ahadi, L. Dong, S. Stemmer, and J. W. Harter, Ferroelectric enhancement of superconductivity in compressively strained SrTiO_3 films, Physical Review Materials **3**, 091401 (2019).
- [105] D. Jena, R. Page, J. Casamento, P. Dang, J. Singhal, Z. Zhang, J. Wright, G. Khalsa, Y. Cho, and H. G. Xing, The new nitrides: Layered, ferroelectric, magnetic, metallic and superconducting nitrides to boost the gan photonics and electronics eco-system, Japanese Journal of Applied Physics **58**, SC0801 (2019).
- [106] C. W. Rischau, X. Lin, C. P. Grams, D. Finck, S. Harms, J. Engelmayer, T. Lorenz, Y. Gallais, B. Fauque, J. Hemberger, *et al.*, A ferroelectric quantum phase transition inside the superconducting dome of $\text{Sr}_{1-x}\text{Ca}_x\text{TiO}_3$, Nature Physics **13**, 643 (2017).
- [107] S. Hameed, D. Pelc, Z. W. Anderson, A. Klein, R. Spieker, L. Yue, B. Das, J. Ramberger, M. Lukas, Y. Liu, *et al.*, Enhanced superconductivity and ferroelectric quantum criticality in plastically deformed strontium titanate, Nature Materials **21**, 54 (2022).
- [108] K. Takahashi, M. Gabay, D. Jaccard, K. Shibuya, T. Ohnishi, M. Lippmaa, and J.-M. Triscone, Local switching of two-dimensional superconductivity using the ferroelectric field effect, Nature **441**, 195 (2006).
- [109] C. Q. Sun, W. Zhong, S. Li, B. Tay, H. Bai, and E. Jiang, Coordination imperfection suppressed phase stability of ferromagnetic, ferroelectric, and superconductive nanosolids, The Journal of Physical Chemistry B **108**, 1080 (2004).
- [110] A. Crassous, R. Bernard, S. Fusil, K. Bouzehouane, J. Briatico, M. Bibes, A. Barthélemy, and J. E. Villegas, $\text{BiFeO}_3/\text{yBa}_2\text{Cu}_3\text{O}_{7-\delta}$ heterostructures for strong ferroelectric modulation of superconductivity, Journal of Applied Physics **113**, 024910 (2013).
- [111] K. Ahadi, L. Galletti, Y. Li, S. Salmani-Rezaie, W. Wu, and S. Stemmer, Enhancing superconductivity in SrTiO_3 films with strain, Science advances **5**, eaaw0120 (2019).
- [112] M. Gabay and J.-M. Triscone, Ferroelectricity woos pairing, Nature Physics **13**, 624 (2017).
- [113] F. J. Wuilleumier, Yvette Cauchois and her contribution to X-ray and inner-shell ionization processes, in *AIP Conference Proceedings*, Vol. 652, pp. 30–49.
- [114] Y. Cauchois and N. Mott, CXVI. The interpretation of X-ray absorption spectra of solids, The London, Edinburgh, and Dublin Philosophical Magazine and Journal of Science **40**, 1260 (1949).
- [115] A. Bianconi, Ugo Fano and shape resonances, in *AIP Conference Proceedings*, Vol. 652 (American Institute of Physics, 2003) pp. 13–18.
- [116] Y. Cauchois, C. Bonnelle, and G. Missoni, Rayonnement electromagnetique-premiers spectres X du rayonnement dorbite du synchrotron de Frascati, Comptes Rendus Hebdomadaires des Seances de L'Academie des Sciences **257**, 409 (1963).